XRES from an $[Er_{20}|Tb_5]$ Superlattice

J. Voigt,[1] D. Wermeille,[2] T. Brückel[1]
[1]Institute of Solid State Research, Research Centre Jülich, Jülich, Germany
[2]Ames Laboratory and Department of Physics and Astronomy, Iowa State University, Ames, IA, U.S.A.

Introduction

The magnetism of nanostructured materials fascinates scientists because of its relevance to understanding the influence of surfaces, interfaces, and electronic confinement. Applications of these materials in electronic devices open a revolutionary window because of the spin nature of their electrons.

Artificial superlattices containing rare-earth materials exhibit a variety of astonishing magnetic phenomena [1 and references therein]. Most noteworthy is the effect of interlayer exchange coupling (i.e., the formation of a coherent magnetic structure), even though nonmagnetic spacer layers separate the magnetic layers. Introducing spacer layers with a different magnetic structure leads to even more complex phases, as shown in Ref. 2.

The ground state of the pure elements is mainly determined by the subtle balance among the RKKY interaction, crystal field anisotropy, and magnetoelastic energy [3]. In a superlattice containing Er and Tb, the anisotropies are fairly different. Bulk Tb exhibits two ordered magnetic phases. For both ordered states, the magnetic moments are aligned within the basal plane of the hexagonal lattice because of the strong crystal field anisotropy. The helix phase is stable between 230 and 220K. Below 220K, the magnetic structure is simply ferromagnetic. Er, in contrast, shows a series of different ordered phases below 81K, with a preferred orientation along the c-direction. At temperatures below 20K, the c-axis component becomes ferromagnetic, while the basal plane component remains in a modulated structure.

The pure materials show strong magnetostriction when they become ferromagnetic, exemplifying the influence of the magnetoelastic energy. It is evident that the epitaxial strains in a superlattice affect the magnetic structure. In a superlattice containing Er and Tb, magnetic proximity effects and the competing anisotropies affect the magnetic ground state. In our work, we are investigating the magnetic structure of a series of [Er|Tb] superlattices with different compositions in order to systematically study the influence of the different contributions.

Methods and Materials

The superlattice was grown by molecular beam epitaxy (MBE) on a sapphire substrate. The recipe given in Ref. 1 was followed to evaporate a buffer containing 250 Å of Nb and 600 Å of Y onto the substrate, providing a smooth (0001) surface of Y. The growth conditions were optimized by *in situ* low-energy electron diffraction (LEED) and Auger electron spectroscopy (AES). At a substrate temperature of 330K, the surface mobility was good enough to yield single crystalline surfaces and to suppress interdiffusion. The superlattice contains 150 bilayer units, composed of 20 atomic layers of Er and 5 atomic layers of Tb. Finally, to protect the sample against oxidation, a 250-Å Y cap layer was evaporated.

The magnetic structure of the sample was determined by neutron diffraction. Below 150K, a basal plane helix (H) was observed. Below 80K, the c-axis component is aligned with the same modulation vector as is the basal plane component, referred to as tilted helix (TH). Ferromagnetic phases appear below 40K for the basal plane (FM in Fig. 1) and below 20K for the c-component (cone).

To study the magnetic behavior of the film specific elements, we measured the x-ray resonant exchange scattering (XRES) from the specimen. When the energy of the incoming photons was tuned to the absorption edge of the elements, the resonant enhancement of the magnetic scattering provided information about the magnetic state of the respective material only. The

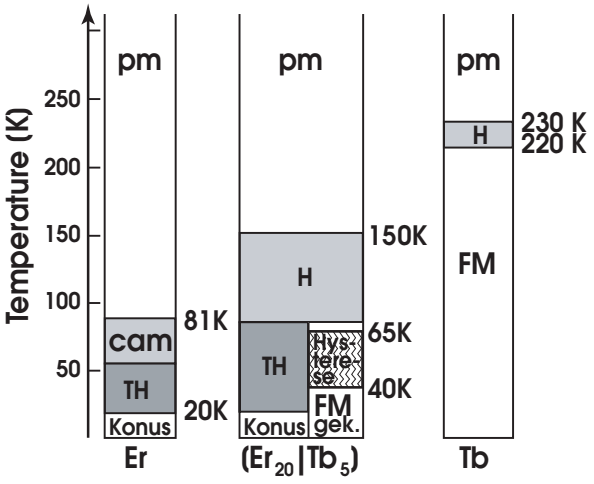

FIG. 1. Schematic phase diagram for the pure elements and the $[Er_{20}|Tb_5]$ superlattice as deduced by neutron scattering. (Abbreviations are described in the text.)

sample was mounted to a closed-cycle cryostat. The sample temperature could be varied between 6 and 300K at an accuracy of better than 1K. A vertical scattering geometry was chosen. In order to suppress the dominant charge scattering, the polarization of the scattered photons was analyzed. We chose a vertical scattering geometry to analyze the polarization in σ-π' geometry (i.e., we measured the component of the scattered light that was rotated by the resonant magnetic scattering process). In contrast, charge scattering left the polarization state unchanged. The charge scattering was suppressed by 95% at the Er L_{III} edge and by more than 99% at the Tb L_{III} edge. The high efficiency at the Tb edge could be achieved by using an Al(222) crystal. At the Er edge, we employed a pyrolitic graphite crystal using the (0006) reflection.

Results

We performed linear scans in reciprocal space along the (000Q_z) direction (the growth direction of the superlattice). The magnetic modulation propagates along the same direction. The normalized intensity as a function of the Q_z component of the scattering vector is shown in Figs. 2 and 3 for measurements at the Er and Tb L_{III} edges, respectively. At the Tb edge, the XRES signal could be observed in the vicinity of the (0002) peak because of the more efficient polarization analysis. As the charge scattering decreases with increasing Q_z, the XRES can be distinguished at the Er edge only around the (0004) central Bragg peak.

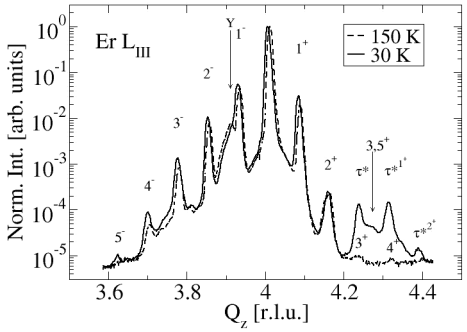

FIG. 2. XRES as a function of Q_z at the Er L_{III} edge (E = 8.361 keV) in the paramagnetic state (150K) and in the magnetically ordered state (30K). (Nomenclature is explained in the text.)

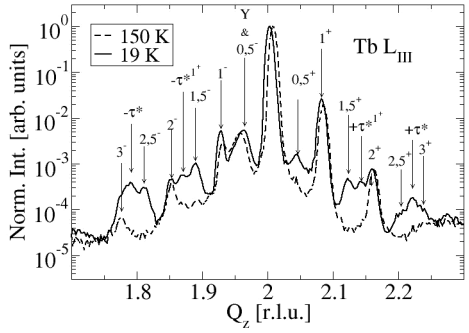

FIG. 3. XRES as a function of Q_z at the Tb L_{III} edge (E = 8.361 keV) in the paramagnetic state (150K) and in the magnetically ordered state (30K). (Nomenclature is explained in the text.)

The reflections can be classified as follows:

1. $Q_z = \frac{4\pi l}{c} \pm \frac{2\pi l'}{D}$

   These reflections exist only at high temperatures because of the epitaxial growth (hexagonal lattice with averaged lattice constant convoluted with the superlattice of periodicity D). The index l' is given in Figs. 2 and 3.

2. $Q_z = \frac{4\pi l}{c} \pm \frac{\Phi \pm 2\pi l'}{D} = \frac{4\pi l}{c} \pm \left(\tau^* \pm \frac{2\pi l'}{D} \right)$

   These additional reflections appear at low temperatures because of the magnetic modulation. Φ denotes the accumulated phase across one bilayer. $\tau^* = \Phi/D$ denotes the magnitude of the respective modulation vector.

3. $Q_z = \frac{4\pi l}{c} \pm \frac{2\pi(2l'-1)}{2D}$

   These half-integer reflections are present at low temperatures where the antiferromagnetic coupling of ferromagnetically ordered layers sets in. The reflections are indexed in Figs. 2 and 3 by $(2l' - 1)/2$.

These are the same type of reflections as those measured by neutron scattering. The magnetic origin of the signal is confirmed by the energy dependence, which shows a resonant behavior for both type 2 and 3 reflections (Figs. 4 and 5).

Since XRES from Er and Tb measures mainly the polarization of the 5d conduction electrons [4, 5], we observed identical Fourier components within this band, since the data show the same qualitative features for both energies. This holds true for the modulated magnetic structure, which is similar to the phases found in bulk Er, and for the basal plane ferromagnetic order, as found in bulk Tb. A strong thermal hysteresis was found for the ferromagnetic ordering. Upon cooling, it sets the ordering at about 40K, and the ordering persists upon heating to 65K.

Discussion

The XRES experiment at the LIII edge mainly probes the density of states in the 5d conduction band. Since the RKKY interaction between localized 4f states leads to exchange-splitting of the conduction bands, the

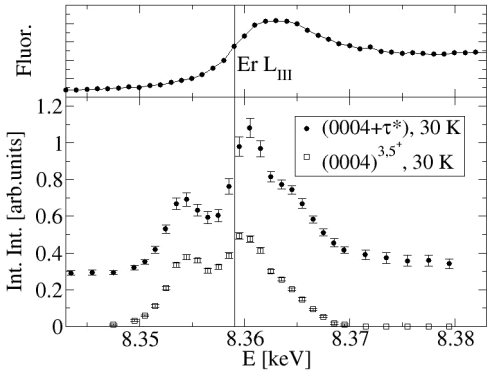

FIG. 4. Integrated intensity of the (0004 + τ^*) and the $(0004)^{3.5+}$ reflections as a function of energy close to the Er L_{III} edge. The position of the edge is defined by the fluorescence yield, shown on top of the figure.

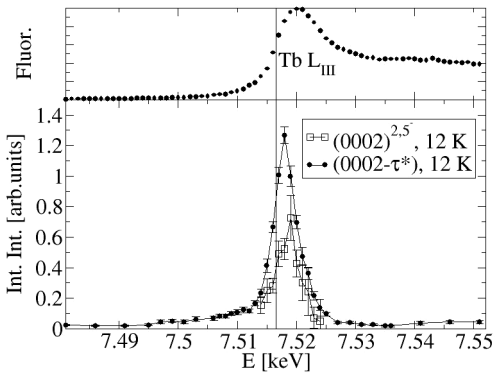

FIG. 5. Integrated intensity of the (0002 - τ^*) and the $(0002)^{2.5-}$ reflections as a function of energy close to the Tb L_{III} edge. The position of the edge is defined by the fluorescence yield, shown on top of the figure.

resonant scattering is sensitive to the magnetic state.

The long-range-ordered magnetic structures as revealed by neutron diffraction lead to coherent spin density waves inside both conduction bands.

Despite the tiny amount of material in the superlattice, a clear XRES signal can be detected. The high instrumental resolution allows the distinction between overlapping reflections, which cannot be resolved uniquely by neutron diffraction. In addition, the correlation length can be estimated to a higher accuracy, since the broadening due to instrumental resolution is negligible.

The XRES data clearly show the coherent spin polarization of the conduction electrons throughout the multilayer. A superlattice conduction band structure is formed, in which the spin polarization develops with identical Fourier components in both elements. It causes the effects of magnetic proximity (i.e., the change of phase-transition temperatures and the formation of new magnetic phases). This is one of the first studies to directly observe the coupling via conduction band electrons. In that way, it exemplifies the power of using XRES to study nanostructured materials in the future.

The tendency to a coherent magnetic structure throughout the superlattice is opposed by the competing anisotropies inside the Er and Tb layers. This leads to the strong thermal hysteresis and to a temperature-dependent correlation length, deduced from the width of the reflections.

Acknowledgments

Use of the APS was supported by the U.S. Department of Energy (DOE), Office of Science, Office of Basic Energy Sciences, under Contract No. W-31-109-ENG-38. The MU-CAT sector at the APS is supported by the DOE Office of Science through Ames Laboratory under Contract No. W-7405-ENG-82.

References

[1] C.F. Majkrzak et al., Adv. Phys. **40**, 99 (1991).
[2] R.A. Cowley, J. Magn. Magn. Mater. **177-181**, 1156 (1998).
[3] J. Jensen and A.R. Macintosh, *Rare Earth Magnetism* (Oxford University Press, 1991).
[4] M.K. Sanyal et al., Phys. Rev. B **49**, 1079-1085 (1994).
[5] S.C. Perry et al., J. Phys.: Cond. Mat. **10**(9), 1951-